

Directional association of TeV to PeV astrophysical neutrinos with active galaxies hosting compact radio jets

A. V. PLAVIN,^{1,2} Y. Y. KOVALEV,^{1,2,3} YU. A. KOVALEV,¹ AND S. V. TROITSKY⁴

¹*Astro Space Center of Lebedev Physical Institute, Profsoyuznaya 84/32, 117997 Moscow, Russia*

²*Moscow Institute of Physics and Technology, Institutsky per. 9, Dolgoprudny 141700, Russia*

³*Max-Planck-Institut für Radioastronomie, Auf dem Hügel 69, 53121 Bonn, Germany*

⁴*Institute for Nuclear Research of the Russian Academy of Sciences, 60th October Anniversary Prospect 7a, Moscow 117312, Russia*

(Received 2020 September 18)

Submitted to ApJ

ABSTRACT

We have shown recently that high-energy neutrinos above 200 TeV detected by IceCube are produced within several parsecs in the central regions of radio-bright active galactic nuclei (AGNs). To independently test this result and to extend the analysis to a wider energy range, we use here public data for all energies from seven years of IceCube observations. The IceCube point-source likelihood map is analyzed against positions of AGNs from a large complete sample selected by their compact radio flux density. The latter analysis delivers 3.0σ significance with the combined post-trial significance of both studies being 4.1σ . The correlation is driven by a large number of AGNs. Together with fainter but physically similar sources not included in the sample, these radio-bright quasars may explain the entire IceCube astrophysical neutrino flux as derived from muon-track analyses. The neutrinos can be produced in interactions of relativistic protons with X-ray self-Compton photons in parsec-scale AGN jets.

Keywords: neutrinos – galaxies: active – galaxies: jets – quasars: general – radio continuum: galaxies

1. INTRODUCTION

The origin of high-energy astrophysical neutrinos, being detected for years by the IceCube experiment, remains unknown. Observational data do not support some of the earlier expectations and put forward more puzzles thus complicating theoretical implications. While active galactic nuclei (AGNs) were considered as a probable class of the neutrino sources since the very early days of the multimessenger astronomy (Berezinsky 1977; Eichler 1979; Berezinskii & Ginzburg 1981), no statistically significant association of neutrino events with gamma-ray loud AGNs has been found (see, e.g., Aartsen et al. 2017a; Neronov et al. 2017; Palladino & Vissani 2017; Righi et al. 2019; Huber 2019; Aartsen et al. 2020a). In addition, gamma-ray blazars are

not numerous, and the lack of observation of individual bright sources puts strong constraints on this scenario, cf. Yuan et al. (2020); Neronov & Semikoz (2020); Capel et al. (2020). This is however in contrast with the association of a single high-energy neutrino event (IceCube Collaboration et al. 2018a) with a gamma-ray flare of an AGN TXS 0506+056 and of an excess of low-energy events from the same direction (IceCube Collaboration et al. 2018b). Detailed discussions of the AGN models of astrophysical neutrinos can be found, e.g., in reviews by Böttcher (2019); Cerruti (2019), while more general descriptions of IceCube observations and of various scenarios of the neutrino origin are presented, e.g., by Ahlers & Halzen (2018); Palladino et al. (2020).

Recently, we found a 3.1σ -significant association of track-like events with estimated neutrino energies $E_\nu > 200$ TeV from publicly available IceCube lists with radio-bright compact parsec-scale cores of AGNs (Plavin et al. 2020). The key point in this observation was the use of very-long-baseline radio interferometry (VLBI) capa-

ble to resolve central parsecs of AGN, in particular of a complete full-sky flux-density-limited sample of VLBI-selected extragalactic sources. We found that AGNs whose positions in the sky coincide, up to the measurement errors, with arrival directions of neutrino events have stronger parsec-scale radio cores than the rest of the sample, with the post-trial probability of random coincidence of $2 \cdot 10^{-3}$. Moreover, on average, these potential neutrino sources exhibited radio flares at the time of the neutrino arrival as measured by the RATAN-600 radio telescope.

This observation reopened the possibility to explain the bulk of high-energy astrophysical neutrinos by AGNs, at the same time evading constraints from the lack of both gamma-ray associations and significant individual point-like neutrino sources. In addition, this result gives physical grounds to the association of TXS 0506+056, a quasar bright both in radio and in gamma rays, with the IceCube 170922A neutrino event (IceCube Collaboration et al. 2018a), which otherwise looks orphan in the absence of other similar neutrino/gamma-ray coincidences.

After results of the analysis were published by Plavin et al. (2020), new important observational data became available. The IceCube Collaboration has released seven-year (2008–2015) public data adopted for the search of point-like neutrino sources (IceCube Collaboration 2020). The main task of our present work is to use these newly released neutrino data to search for association with VLBI-selected AGNs from the sample used by Plavin et al. (2020). Besides the possibility to perform the test of the conjectured neutrino – radio AGN association with independent data, this is important for the following reason. Though the events above 200 TeV, used in the previous analysis, have relatively high probability of being astrophysical, they represent the very tail of the IceCube spectrum, cf. Stettner (2019); IceCube Collaboration et al. (2020a), while the data we use here are dominated by neutrinos of considerably lower, down to TeV, energies. Production of TeV and sub-PeV neutrinos in AGN requires different physical conditions, hence the present study provides additional nontrivial constraints on theoretical models.

The rest of the paper is organized as follows. In Section 2, we describe the public IceCube (Section 2.1) and VLBI (Section 2.2) data used in the study. Section 3 presents the analysis of these data and its results. In Section 4, we compare these results with those of Plavin et al. (2020) and derive a combined statistical significance of the two studies. Section 5 estimates the neutrino flux produced by AGNs and puts it into a wider context. Section 6 discusses theoretical implications of

our results. In Section 7, we briefly summarize our findings and discuss ongoing and future observations aimed to explore and refine the results of this study.

2. DESCRIPTION OF THE UTILIZED DATA

2.1. IceCube data

The IceCube Collaboration routinely performs dedicated searches for point-like neutrino sources as the data are accumulated (Aartsen et al. 2017b, 2019a, 2020b, 2019b, 2020a), also jointly with ANTARES (Albert et al. 2020). No significant point source was found: in all cases, the post-trial significance is below 3σ . The most significant source from a predefined catalog is a star-forming Seyfert galaxy NGC 1068 (2.9σ post-trial with 10 years of track-like data, Aartsen et al. 2020a). However, the best-fit spectrum of this putative source is very soft and the total flux is way too large, suggesting a positive fluctuation in the atmospheric background. Stacking analyses of radio-selected sources were not performed in those works.

The ten-year IceCube track data, as well as cascade data, have not been publicly released yet. However, the track data covering seven years (2008–2015) used in the analysis of Aartsen et al. (2017b), has been published (IceCube Collaboration 2020) in the form of pre-trial local p -values on a grid of pixels covering the entire sky. We denote the provided negative logarithms of local p -values as $L = -\log p$, so that they are not confused with statistical p -values computed in the following sections for the present analysis. In our analysis we treat L as a measure of detected direction-dependent neutrino emission: larger L corresponds to a higher probability that a point source of astrophysical neutrinos is located in the given direction in the sky.

The map of L values is based on 712830 detected events, but does not explicitly contain the information on their individual properties. These L are based on the likelihood of the model assuming an astrophysical neutrino source in a given direction with a power-law spectrum. Therefore they accumulate information about arrival directions and energies of neutrinos in an area of the sky over the entire observational period of seven years. Note that the probability of an event being astrophysical and not caused by the atmospheric background grows with energy, and this dependency was included in the calculation of the likelihood (Aartsen et al. 2017b). The likelihood is further influenced by the neutrino energies through the energy-dependent angular resolution and sensitivity of IceCube. The effective area, reported in IceCube Collaboration (2020), is generally larger for more energetic particles, and steeply falls below ~ 10 TeV. The angular resolution is roughly 0.5° at

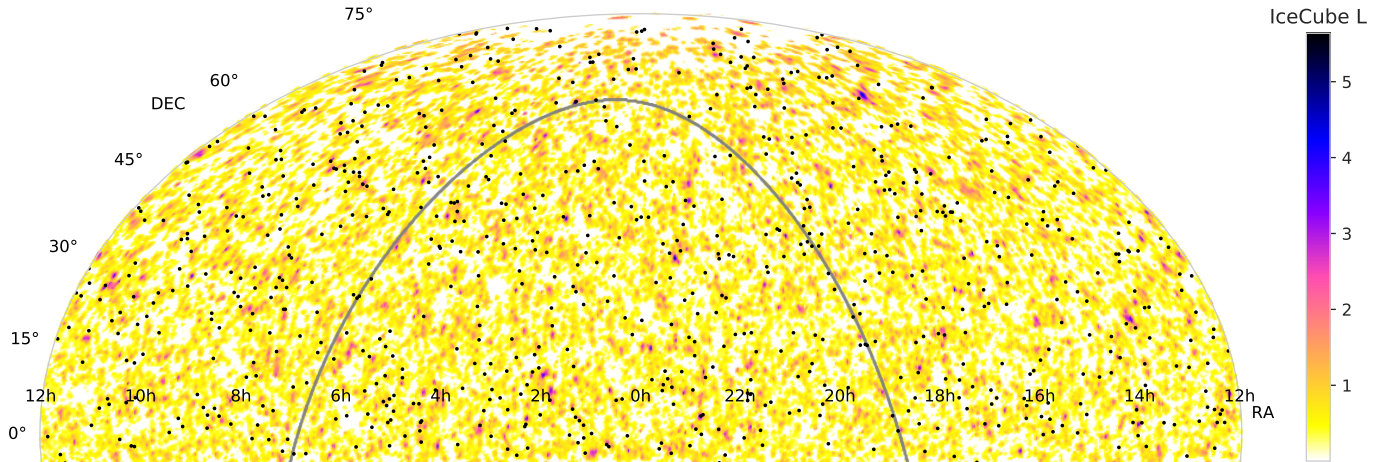


Figure 1. The sky map of the IceCube local p -value logarithms denoted as L . All sky north of $\delta = -5^\circ$ is displayed in equatorial coordinates. Darker areas with larger L indicate higher probabilities to have an astrophysical neutrino point source in this direction, see Section 2.1. AGNs from the complete 8 GHz VLBI sample down to the flux density of 0.33 Jy are shown by black dots. The grey line represents the Galactic plane.

energies above 100 TeV, and increases for less energetic neutrinos. The distance between neighbouring pixels in the grid is about 0.1° , several times smaller than the highest achieved resolution; therefore we do not perform any additional oversampling or interpolation. We drop the Southern sky (declination $\delta < -5^\circ$) from our analysis due to a heavily degraded sensitivity of IceCube to astrophysical neutrinos in that range in the muon-track channel; this effect is discussed in (Aartsen et al. 2017b). Further in this paper we refer to the $\delta > -5^\circ$ range as the Northern sky. This area of the map is influenced by 422791 individual detection events (Aartsen et al. 2017b).

In a part of our work we additionally utilize the largest published dataset of individual IceCube events that however covers only three years, 2010-2012 (IceCube Collaboration 2018). It contains 334677 events, and 196316 of those are in the Northern sky. Each event in the catalog is described by the arrival direction in the sky, statistical uncertainties of this direction, and the estimated particle energy. We remove detections whose 90% containment area on the celestial sphere is larger than 10 deg^2 , which leaves us with 114799 events north of $\delta = 5^\circ$ out of the original 196316.

2.2. VLBI Observations of AGNs

For our analysis we use the same 8 GHz VLBI data as in Plavin et al. (2020) that are compiled in the Astrogeo¹ database. These observations include geodetic VLBI programs (Petrov et al. 2009; Pushkarev & Kovalev 2012; Piner et al. 2012), the Very Long Baseline

Array (VLBA) calibrator surveys (VCS; Beasley et al. 2002; Fomalont et al. 2003; Petrov et al. 2005, 2006; Kovalev et al. 2007; Petrov et al. 2008; Petrov 2017; Gordon et al. 2016), and other 8 GHz global VLBI, VLBA, EVN (the European VLBI Network), LBA (the Australian Long Baseline Array) observations (Petrov et al. 2011a; Petrov 2011; Petrov et al. 2011b; Petrov 2012, 2013; Schinzel et al. 2015; Shu et al. 2017; Petrov et al. 2019; Petrov 2020; Popkov et al. 2020). The AGN positions are determined from these observations and presented within the VLBI-based Radio Fundamental Catalogue² (RFC). We use the latest available version to date, RFC 2020b. The catalog includes a complete sample of AGNs limited by the 8 GHz flux density integrated over VLBI images $S_{8\text{GHz}} \geq 150 \text{ mJy}$. This complete sample contains 3411 objects, and 1938 of those are located north of $\delta = -5^\circ$.

In our analysis, we use the aforementioned flux densities of AGNs, call them “VLBI flux densities” throughout the paper, and denote as S in equations. The majority of the AGNs comprising our sample are strongly Doppler-boosted, and their flux density is dominated by the emission of the apparent parsec-scale jet base, the core (e.g., Kovalev et al. 2005; Pushkarev & Kovalev 2012). For the sources with multiple VLBI observations, the average flux density of all the measurements is used in the analysis. The median number of VLBI observations at 8 GHz for a source is 5, the maximal is more than 150.

² <http://astrogeo.org/rfc/>

¹ <http://astrogeo.org/vlbi.images/>

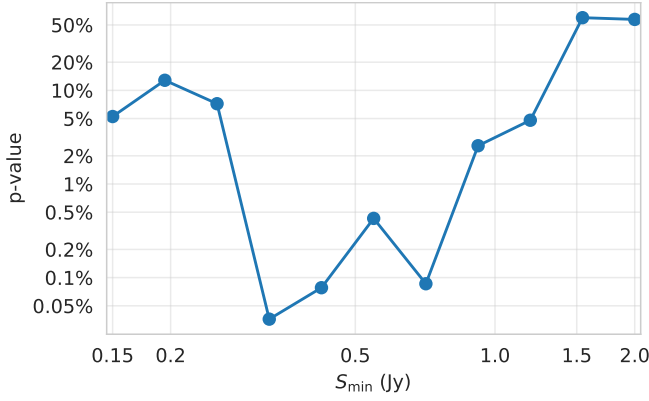


Figure 2. Pre-trial p -values for a range of VLBI flux density cutoffs. The threshold values S_{\min} split the interval 0.15-2 Jy into ten parts uniformly in log-scale. The lowest p -value of $4 \cdot 10^{-4}$ is attained for the threshold of 0.33 Jy.

3. CORRELATION OF RADIO-BRIGHT AGNS AND TIME-INTEGRATED NEUTRINO FLUX

We address here the question whether radio-bright VLBI-selected AGNs tend to produce neutrinos detected by IceCube. We utilize the time-aggregated likelihoods of astrophysical neutrino sources from IceCube (Section 2.1) together with the average historic VLBI flux density of AGNs (Section 2.2). Appendix A motivates and discusses L -value normalization, L_{norm} , which we use below.

We select all AGNs with the VLBI flux density higher than a threshold S_{\min} determined below, extract L_{norm} values at their positions, and take the median of these values as the test statistic. Then we test whether the value of this statistic is higher than could arise by chance: the entire IceCube L map is repeatedly rotated in Right Ascension 10^5 times by random amounts, yielding the null distribution. The pre-trial p -values are calculated based on this. See our previous study (Plavin et al. 2020) for motivation and details of this testing procedure. The trial S_{\min} thresholds are taken from the interval [150 mJy; 2 Jy] split into ten parts evenly in logarithmic scale. Here the lower bound is dictated by the sample completeness (Section 2.2), and the upper bound is chosen so that at least 40 AGNs remain in the selection. The p -values for each threshold are shown in Figure 2: the minimum of $p = 4 \cdot 10^{-4}$ is achieved for $S_{\min} = 0.33$ Jy. Then the global post-trial p -value is calculated following the motivation and procedure detailed in Plavin et al. (2020). It represents the chance probability for the median L_{norm} at bright AGN positions to be as high as actually observed. This probability is found to be $3 \cdot 10^{-3}$, which corresponds to the significance of 3.0σ for a normal distribution.

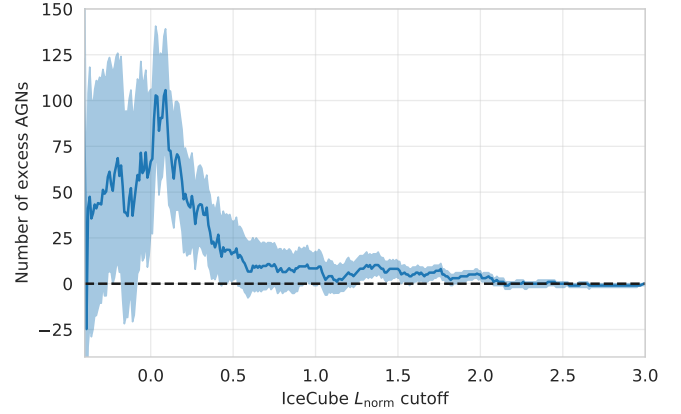


Figure 3. Number of excess AGNs with normalized IceCube L values higher than a given cutoff. The blue line indicates the estimated number itself, and the shaded area represents the 1σ uncertainty. These counts are estimates of how many AGNs are associated with detected neutrinos, if only objects with L_{norm} higher than the cutoff are considered.

The particular value of S_{\min} yielding the minimal p -value is unlikely to bear any specific astrophysical meaning: it represents a trade-off between fewer sources remaining with higher cutoffs, and fainter sources covering larger fractions of the sky at lower thresholds. This trade-off depends on the sensitivity and effective resolution of neutrino telescopes, and the optimal S_{\min} will likely be different for different datasets. However, for the available observational data from IceCube we find that the neutrino-AGN association is dominated by bright AGNs above 0.33 Jy. This value is used in Section 5.2 for rough estimates of the neutrino flux from AGNs.

After having determined with the significance of 3.0σ that an excess of neutrinos is detected from the directions of radio-bright AGNs, we proceed to estimate how many extragalactic objects drive this correlation. For a range of L_{norm} thresholds we count the number of AGNs with L_{norm} at their position in the sky higher than the threshold. Then we subtract the counts obtained in the same way for AGN positions randomly shifted in Right Ascension. These differences yield estimates of the excess of AGNs that are shown in Figure 3. The maximum excess count of 104 ± 32 is achieved for $L_{\text{norm}} > 0.09$. This cutoff value being close to zero and the overall shape of the plot indicate that the majority of neutrino-emitting AGNs have IceCube L values that are not extremely high, but close to their median. Such AGNs can only be distinguished by a statistical approach of this kind, and would be lost in any analysis focused on the brightest regions of the IceCube map.

This maximum excess count can slightly overestimate the true number of responsible AGNs because of fluctuations: this reflects the multiple comparisons prob-

lem. Thus we proceed with a conservative approach. Maxima of the excess are computed for AGN positions randomly shifted in Right Ascension, following the same motivation as above. These maxima are subtracted from the real-positions maximum. The resulting estimate of the detected excess count is 72 ± 23 . We take this as an estimate of the number of AGNs that significantly contribute to the correlation with neutrinos established above. Note that there are likely more neutrino-emitting AGNs, but their neutrino flux is too low to be detected even in this aggregated fashion. Thus the excess counts are expected to go up when more sensitive observations become available. The current values are to be treated as lower limits.

4. SELECTED HIGH ENERGY EVENTS AND THE ALL-SKY ICECUBE MAP: JOINT ANALYSIS

Earlier this year in [Plavin et al. \(2020\)](#) we have shown that AGNs positionally associated with IceCube events above 200 TeV have stronger parsec-scale cores than the rest of the AGN sample. Analysis in the present work is based on IceCube data released after that paper was published, and thus can be considered a largely independent statistical study. Effects explored in this and the previous paper correspond to the same kind of objects, same spatial scales and underlying mechanisms; the main difference is the range of neutrino energies dictated by the available observational data from IceCube.

After the work of [Plavin et al. \(2020\)](#) was published, it has been pointed out (T. Hovatta et al., in prep.) that the IceCube event on 2012-05-15 has the reported energy of exactly 200 TeV. This event was not used in our original analysis due to the strict inequality requirement $E > 200$ TeV. We consider this being non-optimal, and repeat the analysis of [Plavin et al. \(2020\)](#) including this event. The arrival direction of this neutrino is positionally associated with a compact radio-bright quasar 1308+326 (OP 313) that has the average VLBI flux density of 1.9 Jy at 8 GHz. Additionally this AGN experienced a major radio flare peaking around 2012 temporally coincident with the neutrino detection. Including this 200 TeV event slightly increases the post-trial statistical significance obtained in the analysis in [Plavin et al. \(2020\)](#) from 3.1σ ($p = 2 \cdot 10^{-3}$) to 3.4σ ($p = 7 \cdot 10^{-4}$). We use this updated p -value below to improve the completeness of the neutrino-VLBI analysis covering high energy events in 2010-2019. This choice does not affect any of our conclusions.

Further in this section we combine the results of [Plavin et al. \(2020\)](#) and of [Section 3](#) to obtain the joint significance level of the neutrino-AGN association. This combination is justified because each of the two uti-

lized IceCube datasets contains important information not available in the other. The catalog used in [Plavin et al. \(2020\)](#) covers years from 2010 to 2019, contains detailed information about each event such as its direction and energy. However, it lists only high-energy neutrinos that have a high probability to be of astrophysical origin. The analysis in [Section 3](#), conversely, is based on all detected events independently of their energy, but only contains highly aggregated information and covers the period from 2008 to 2015. To perform the combination in the most conservative way possible, we apply a mask to the IceCube map of L (see [Section 2.1](#) for the map details) to remove the contribution of individual neutrinos already accounted in the previous analysis. Specifically, we mask out the pixels that are close to any of the IceCube events earlier than 2016.0 listed in [Plavin et al. \(2020\)](#) with an addition of the 2012-05-15 event discussed above. The closeness threshold is taken equal to the positional errors of those events assuming a 0.5° systematic uncertainty, see [Plavin et al. \(2020\)](#) for discussion. With these regions masked out, the post-trial p -value based on the all-sky map analysis described in [Section 3](#) marginally increases from $3 \cdot 10^{-3}$ to $4 \cdot 10^{-3}$. Finally we follow the Fischer’s method of combining p -values from independent analyses ([Fisher 1925](#)), and obtain the joint probability of chance coincidence $p = 4 \times 10^{-5}$ that corresponds to 4.1σ for a normal distribution.

The physical effects and source regions probed by our analyses of higher- and lower-energy neutrino samples are the same. At the same time, the number of AGNs manifesting themselves as neutrino emitters differs significantly. Neutrinos above 200 TeV are rare: there are only 57 events passing the selection criteria in [Plavin et al. \(2020\)](#). About 35 of them are expected to have an astrophysical origin, and about 10 AGNs from our sample can be currently associated with these events ([Plavin et al. 2020](#)). Those objects are among the brightest or the most flaring radio AGNs in the sky. Lower energy neutrinos are a lot more numerous with 422791 events in the Northern sky contributing to the IceCube map ([Section 2.1](#), [Figure 1](#)). Only a fraction of $3 \cdot 10^{-3}$ of them, that is around 1300, are likely to have an astrophysical origin, cf. [Stettner \(2019\)](#). As illustrated in [Figure 3](#) and deduced in [Section 3](#), about 70 AGNs can already be associated with such neutrinos, even though we cannot reliably list individual sources yet. They constitute a noticeable fraction of the entire compact radio-bright AGN population: there are 1938 AGNs in total within our complete sample in the Northern sky, and 725 of them are brighter than 0.33 Jy, the threshold yielding the minimal p -value in [Figure 2](#).

5. ESTIMATE OF THE NEUTRINO FLUX FROM AGNS

5.1. Counting individual neutrinos in the three-year data

The number of neutrino-associated AGNs alone does not allow us to estimate the neutrino flux produced by them: this requires counting individual detection events instead of AGNs. The all-sky map of IceCube L does not contain enough information to do that. Thus we attempt to derive these counts from a smaller three-year dataset of individual events detected at IceCube (see [Section 2.1](#) and [IceCube Collaboration 2018](#)). Due to a shorter time period of three years compared to seven for the L map, any estimates based on this data are expected to be more noisy.

We count the number of events that have at least one AGN from our complete sample above 0.15 Jy falling within positional uncertainties. This counting is repeated for the real dataset and for randomly-shifted samples, utilizing the same approach as in [Section 3](#). The difference of these counts yields the number of excess neutrinos, i.e. those that are associated with AGNs. This number is 215 ± 134 , which is consistent with zero at a 2σ level. Thus it does not constitute a significant evidence of a neutrino-AGN connection by itself. This could be expected: the dataset is based on fewer observations, and there is more noise at low neutrino energies resulting from the atmospheric background. However, it is still instructive to compare this estimate of number of AGN-associated neutrinos over the three years to the total number of detection events in the Northern sky over this period, 196316. We find that a fraction of $(1.1 \pm 0.7) \cdot 10^{-3}$ of all the detections can be explained by AGNs in our sample. This is around 1/3 of the total amount of astrophysical neutrinos in the three-year dataset, similar to the fraction for $E_\nu > 200$ TeV case ([Plavin et al. 2020](#) and [Section 4](#) here). Additionally we explore the dependence of the excess neutrino count on their energy. This count continues growing till the lowest energies available in the dataset, on the order of 1 TeV, suggesting that many AGN-associated neutrino detections are in the range of 1-10 TeV. These lower-energy events contribute a little to the likelihood L published for the seven-year data set. However, the statistical errors in the estimates based on three years of observations are too large to reliably conclude whether this is the case and to give more precise estimates.

5.2. Neutrino energy flux: seven years of data

Here we present an order-of-magnitude estimate of the total neutrino flux that can be explained by radio-bright compact AGNs. Our observational results in [Section 3](#)

based on the IceCube L map indicate that at least 70 AGNs above 0.33 Jy are associated with neutrinos detected over seven years. This yields a lower limit of 10 detected neutrinos per year coming from the ensemble of bright AGNs with $S > 0.33$ Jy, even if each source only resulted in a single neutrino detection. The L map represents the likelihood of astrophysical-neutrino point source, and thus should be dominated by the contribution from events above 40 TeV ([Stettner 2019](#)). Despite there also exist lower-energy neutrinos associated with AGNs (see [Section 5.1](#)), they get strongly down-weighted here. We take the energy of 40 TeV as a reasonable estimate for a typical event affecting significantly the value of L . The effective area of IceCube at such energies is about 30 m^2 ([Aartsen et al. 2017b](#)). Under these assumptions we obtain a lower limit on the muon neutrino flux from these objects over the entire sky: $F_\nu^{>0.33\text{Jy}} \gtrsim 80 \text{ eV cm}^{-2} \text{ s}^{-1}$. According to [Stettner \(2019\)](#), the total astrophysical muon neutrino flux at energies above 40 TeV is $F_\nu^{\text{total}} \approx 835 \text{ eV cm}^{-2} \text{ s}^{-1}$. Thus our crudely estimated $F_\nu^{>0.33\text{Jy}}$ already constitutes almost 10% of F_ν^{total} . Account of other AGNs from our sample, with lower flux densities down to 0.15 Jy, would result in a value $F_\nu^{>0.15\text{Jy}} \approx (1.5 \dots 2.5) \cdot F_\nu^{>0.33\text{Jy}}$. The coefficient depends on the specific relationship, or lack thereof, between the radio and neutrino fluxes of the AGNs. These estimates show that $F_\nu^{>0.15\text{Jy}}$ makes up for 1/4 of F_ν^{total} . If in fact the 70 associated AGNs emitted multiple neutrinos on average, then this fraction gets proportionally increased. Moreover, some AGNs within our sample might not get associated with neutrinos because they, e.g., fall into an area with a higher IceCube background. Our estimates are effectively lower limits, and the real number of neutrino-AGN associations in the sample may be larger.

The estimates in this subsection and in [Section 5.1](#) are based on very different approaches and observational datasets from IceCube. Yet the results turn out to be similar and qualitatively consistent. Remaining differences, if any, can be explained by different energies effectively contributing to each dataset. Both of the analyses imply that it is possible to explain the entire astrophysical neutrino flux, as it is estimated from muon-track IceCube studies ([Aartsen et al. 2016](#); [Stettner 2019](#)), by AGNs hosting radio-bright parsec-scale jets, without requiring any extreme assumptions. Indeed, many similar radio AGNs are fainter than the flux density limit of our sample, either because of their intrinsic power, or due to geometrical properties of the beamed emission, but in many cases simply because they are more distant. Together they are expected to contribute a major fraction

to the total neutrino flux, though the limitations of the present analysis do not allow to derive it precisely.

5.3. Neutrino luminosity of an AGN

Next we estimate the total power of neutrinos emitted by a typical AGN among those associated with IceCube detections in Section 3. For AGNs brighter than 0.33 Jy, the realistic situation is somewhere in between the two possible opposite scenarios. First possibility is if only 70 of such AGNs emit neutrinos: in this case we found all of them in Section 3. Second is if all 700 bright AGNs emit neutrinos at similar rates, and the 70 associated ones just happened to be detected in the covered time period. Corresponding estimates on the average per-source neutrino flux range from 1/70 to 1/7 neutrinos per year if a single neutrino from each of those AGNs got detected. Adopting the same assumptions regarding neutrino energies and the IceCube effective area as in Section 5.2, we roughly obtain $F_\nu \approx (0.06 \dots 0.6) \text{ eV cm}^{-2} \text{ s}^{-1}$.

Typical VLBI-selected AGNs are located at $z \sim 1$ (Lister et al. 2019). The median jet opening angle is estimated by Pushkarev et al. (2017) as 1.3° and the median relativistic beaming angle is about 5° (see Lorentz factor estimates in Lister et al. 2019). We assume that neutrinos, like photons, are emitted isotropically in the emission region frame. If the region is associated with the jet, then neutrinos are emitted within the angle of about 6° from the jet direction. We derive that the total all-flavour neutrino luminosity of such an AGN is approximately $L_\nu \approx (4 \cdot 10^{42} \dots 4 \cdot 10^{43}) \text{ erg s}^{-1}$. Both estimates are a few orders of magnitude below the typical bolometric luminosity of bright AGNs, $L_{\text{bol}} \sim 10^{45} \text{ erg s}^{-1}$ (e.g., Woo & Urry 2002).

6. PHYSICAL IMPLICATIONS

Together with Plavin et al. (2020), the present study ties the neutrino production to central parsec-scale regions of radio-bright AGN, now with even higher significance and for a wider range of neutrino energies. This gives more constraints on the neutrino production mechanism. High-energy neutrinos may be produced in hadronic (proton-proton, pp) or photohadronic (proton-photon, $p\gamma$) interactions. In bright central parsecs of AGNs, pp interactions are generally suppressed with respect to $p\gamma$ (Sikora et al. 1987), though the degree of the suppression depends on the particle energy (e.g., Inoue et al. 2019). Here we summarize briefly some implications of our results in a phenomenological context. These are the keys to understanding of the actual mechanism of the neutrino production.

1. Association of neutrino arrival directions with VLBI-selected AGN suggests the importance of Doppler-boosted jets in the neutrino sources.

2. Neutrino events have been shown to correlate with radio flares. This motivates the assumption that neutrinos may be produced in the observed jet base.

3. Neutrinos with observed energies from TeVs to several PeV originate in objects of one class, AGN. Within the $p\gamma$ scenario, this requires the presence of target photons with different energies whose values are determined below.

4. Previous studies did not reveal any significant statistical association of neutrinos with GeV gamma-ray emission of AGN, either in a steady state or during flares. This may be explained if the bulk of the GeV photons are emitted in different regions than neutrinos. Target photons for $p\gamma$ interactions may also be not connected with the observed gamma-ray emission.

5. Individual AGNs do not reveal themselves as significant sources in the present data. At the same time, our statistical analysis of the entire sample makes it possible to establish the association and demonstrates that a large number of AGN contribute to the neutrino flux, consistent with the origin of the entire astrophysical neutrino flux in sources of this class.

Though much more studies are required to construct a working quantitative model of the neutrino production, we present here a possible concept which qualitatively explains the observational data.

6.1. A possible neutrino production mechanism

6.1.1. Self-Compton target photons

In the first approximation, the cross section of the $p\gamma$ process is saturated by the Δ -resonance which fixes the product of the energies of the proton and the photon in the blob frame, while the proton energy is always ~ 20 times that of the neutrino, see, e.g., Dermer & Menon (2009). Taking into account the Doppler boosting, one finds that the required blob-frame energies of the target photons are $\sim 100 \text{ eV}$ to 20 keV for 10 TeV to PeV observed neutrinos. These energies are far too high for the external photons from the central engine, except maybe the strongly suppressed tail of the corona emission. We have only studied neutrinos above 200 TeV in Plavin et al. (2020) and could not have made these conclusions.

The observed radio emission is the synchrotron radiation from a population of non-thermal electrons. It is inevitably accompanied (e.g., Dermer & Menon 2009) by the synchrotron self-Compton (SC) radiation, consisting of the same synchrotron photons upscattered to high energies by the same relativistic electrons. The SC photons may or may not dominate the observed flux at high energies, but they are always present. At the same time, the observed GeV – TeV radiation of gamma-ray bright blazars is associated with even more

compact and possibly closer to the central black hole region, as determined, e.g., from the day-scale variability (Aharonian et al. 2006; Hayashida et al. 2015). There, inverse-Compton processes on other, external photons may be important. These photons come from the accretion disk, its hot corona, broad-line region and dust torus. All these emissions are less important at ~ 10 pc from the black hole, where the radio-emitting blobs are typically observed (Pushkarev et al. 2010, 2012). In addition, these external radiations are redshifted in the blob frame, which makes them hardly relevant for the neutrino production there. Contrary, the SC photons have typical energies in the keV–MeV range, as needed.

6.1.2. Accelerated protons

The next ingredient is the population of non-thermal protons with energies up to $\sim 10^{16}$ eV in the blob frame. These energies are easily reached in shocks close to the base of the radio jet if these shocks are mildly relativistic (Bykov et al. 2012; Lemoine & Waxman 2009). These “slow” shocks are expected to be present in the jet launching region (Sironi & Spitkovsky 2009) and are often observed by VLBI close to the jet base as stationary or slow features (e.g., Piner et al. 2012; Jorstad et al. 2017; Lister et al. 2019; Kovalev et al. 2020). In addition, these proton energies can be reached by direct acceleration in the black-hole magnetosphere, cf. the “high-luminosity” regime in Ptitsyna & Neronov (2016). Transfer of these protons to the jet would however require a special mechanism (Neronov et al. 2002). Given the low neutrino luminosity of contributing sources, Section 5.3, the injected power of protons in an individual source does not need to exceed the Eddington power by a large factor.

6.1.3. Complicated neutrino spectrum

The spectral shape and the total neutrino flux from an AGN are directly related to those of the target photons, so the neutrino spectrum from an individual AGN is not power-law. Different AGNs have SC bumps at different energies (e.g., Abdo et al. 2010; Mao et al. 2016), and the study of a complicated population of AGNs is required to predict the overall observed neutrino spectrum. In particular, BL Lacs have higher peak frequencies than radio quasars and are therefore more important for production of neutrinos of lower energies. Note that extreme BL Lacs, also proposed earlier as the source of high-energy neutrinos (Padovani et al. 2016), may have the synchrotron SED peak at the required target-photon energies, but they are much less numerous than the AGN we study here.

6.2. Lack of the gamma-ray associations

Together with neutrinos, gamma rays of the same energy are born in the same $p\gamma$ interactions. They however do not survive because they promptly produce electron-positron pairs on the same target photons, giving a start to the electromagnetic cascade. The energy is transformed to lower-energy gamma rays until the pair production becomes impossible because of the threshold, see e.g. Dermer & Menon (2009). Even for the guaranteed target photons required to produce a neutrino, the cascade stops at $\sim 7 \times 10^{-6} E_\nu$ in the observer’s frame. For observed neutrino energies $\lesssim 150$ TeV, the observed photon energy falls below 1 GeV so the corresponding emission is hardly observable by Fermi LAT. The presence of higher-energy photons in the source moves the cascade photons further into the MeV band. There, individual measurements of the AGN flux are mostly absent. Even when the interpolation between keV and GeV is possible, it is not clear which part of the flux comes from the compact jet observed by VLBI and which — from the central engine. Results of future missions aimed at the (sub)MeV astronomy, e.g., eASTROGAM (de Angelis et al. 2018), would be important for obtaining refined quantitative predictions about the neutrino emission. Note, however, that for many sources this contribution to the gamma-ray luminosity is subdominant because the neutrino luminosity, and hence the cascade-photon luminosity, is much smaller than the bolometric photon luminosity of the source, often saturated by hard gamma-ray emission. Together with the strong cosmological evolution of radio AGNs (Smolčić et al. 2009, 2017), this relaxes (Neronov & Semikoz 2020) standard constraints on neutrino-emitting quasars from non-observation of individual sources.

7. SUMMARY

Central parsecs of radio-bright AGNs were shown previously (Plavin et al. 2020) to be associated with astrophysical neutrinos above 200 TeV detected by IceCube. In this work, we analysed newly available information about lower energy muon-track events from 2008–2015. We demonstrated that the association holds for the entire range of energies studied by IceCube, from TeVs to PeVs. The combined post-trial significance of directional correlations found in two independent analyses, at lower and higher energies, is 4.1σ . Temporal correlation of neutrinos with AGN radio flares, found by Plavin et al. (2020) for $E_\nu > 200$ TeV, was not studied at lower energies due to the lack of public information about arrival times of individual IceCube events.

Extension of the neutrino-AGN association to lower energies changes our understanding of the neutrino production mechanism: higher-energy target photons are

required to produce lower-energy neutrinos in the py interactions, which is the most probable channel of neutrino production in AGNs. In radio-loud AGNs these target photons may be provided by the X-ray self-Compton radiation which inevitably accompanies the synchrotron radiation of non-thermal electrons observed in the radio band from the parsec-scale jet. High-energy neutrino emission and gamma radiation may be to an extent independent: they may be produced in different zones of the central parsecs in the AGN. This explains the lack of association between gamma-ray loud AGN and IceCube neutrinos reported in numerous previous studies.

The association we report here was found on statistical and not event-by-event grounds. It implies that the sources are numerous and most of them do not stand out individually in the seven-years IceCube sample. We expect that even in future studies with larger statistics, any analysis focused only on the brightest spots in the neutrino map would miss most of the sources. Many actual neutrino sources still remain outside of our flux-limited sample, including distant or less beamed AGNs. Neutrino luminosity of an individual source is orders of magnitude lower than its bolometric photon luminosity. Overall, we explain at least 1/4 of the astrophysical muon neutrino flux, derived from IceCube track data (Stettner 2019), by the VLBI-selected AGNs brighter than 0.15 Jy. This is consistent with the entire neu-

trino flux being produced in central parsecs of radio-bright AGNs. However, cascade observations may indicate (IceCube Collaboration et al. 2020b) that the flux may be higher at dozens of TeV, and this excess may be associated with a different component (Palladino & Vissani 2016; Ahlers & Halzen 2018).

Future studies will help to verify and clarify the relation between radio quasars and high-energy neutrinos. Results of the present work can be tested with the full collected IceCube data set. Since 2020, IceCube alerts are followed by immediate radio observations by VLBA and RATAN-600. Independently, a set of probable high-energy neutrino emitters is continuously monitored by the same instruments. In the nearest future, the study will be extended to Baikal-GVD (Avrorin et al. 2011) neutrino candidate events. Further ahead, KM3NeT (Katz 2006) in neutrinos and eASTROGAM (de Angelis et al. 2018) in MeV gamma-rays will supplement these studies with important multimessenger information.

ACKNOWLEDGMENTS

We thank Andrei Bykov and Bair Shaibonov for helpful comments and discussions. This work is supported by the Ministry of science and higher education of Russian Federation under the contract 13.1902.21.0005. This research has made use of NASA’s Astrophysics Data System.

Facilities: IceCube neutrino observatory, VLBA, EVN, LBA.

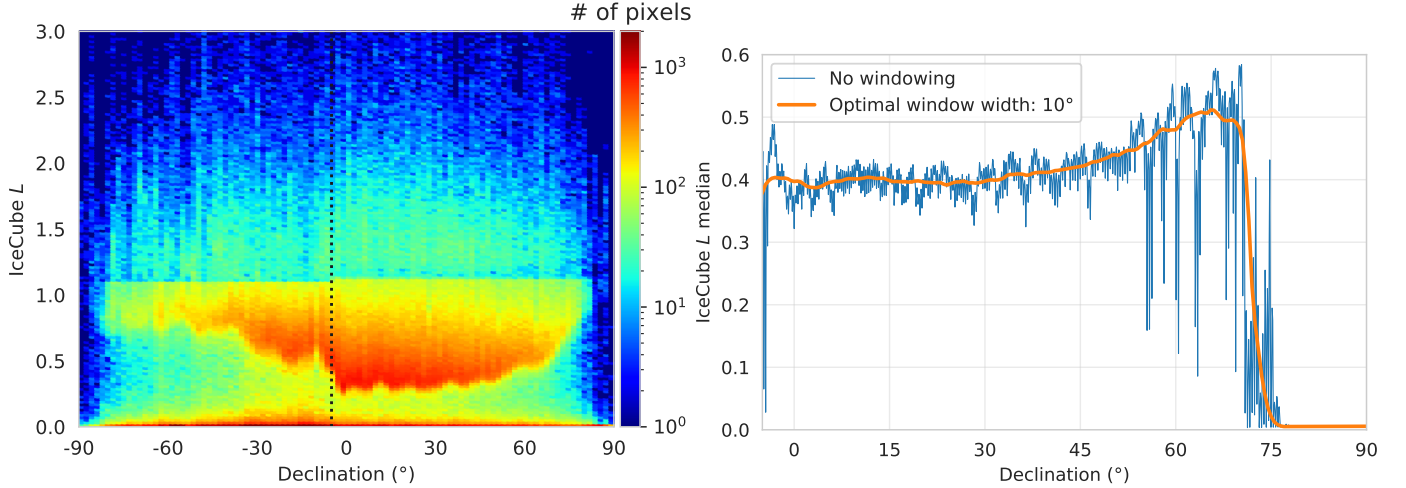
APPENDIX

A. ICECUBE ALL-SKY LIKELIHOOD MAP

Our statistical analysis is based on the IceCube sky map of L values that represent the neutrino point-source detection significance, as mentioned in Section 2.1. We have noticed certain features of the value distribution in this map, and briefly discuss them in this section. Additionally, we attempt to minimize an effect they might have on the analysis.

The histogram of L values across the full range of declinations is shown in the left panel of Figure 4. A prominent feature in this histogram is the abrupt jump around $L \approx 1$: values of L just below the cutoff occur about an order of magnitude more often than L values immediately above. This jump is present for all declinations outside of narrow polar regions, and the cutoff value differs between the northern ($\delta > -5^\circ$) and the southern sky ($\delta < -5^\circ$). We acknowledge that such a peculiarity is present in the L value distribution, but believe that it does not affect our study in any meaningful way. We only utilize the Northern sky, as justified in Section 2.1, and the jump of the L distribution stays constant in this declination range.

The right panel of Figure 4 presents the median value of L for each declination. As apparent from this plot, the typical values of L are highest at declinations around 60° - 70° . If taken at a face value, this effect would indicate that more astrophysical sources stand out from the background at these high declinations. However, the effective sensitivity of IceCube is the highest within $\delta \in [-5, 45]^\circ$ (Aartsen et al. 2017b). The increased L values further to the north should be treated with care. To reduce their effect on any further analysis as conservatively as possible, we first perform a median filtering (running median) on the L values with respect to declination. The window width of the filter is chosen from values between 0° and 30° in steps of 1° by minimizing the mean absolute error via a



(a) Two-dimensional histogram of IceCube L distribution for each declination in the sky. Color indicates the number of pixels at each declination having the corresponding values of L . The total number of pixels is 3145728; less than 0.1 % of them have $L > 3$ and are not shown in this histogram. The region to the right of the vertical dashed line, $\delta > -5^\circ$, is used in our analysis.

(b) Median filtering of the L values with respect to the declination. The blue line marks the median for each individual declination, i.e. each row of pixels in the map, separately. The orange line corresponds to the median computed with the optimal window width of 10° around each declination value.

Figure 4. Illustration of the L distribution in the IceCube seven year sky map.

cross-validation approach; the optimal value turned out to be 10° . The filtered L_{med} are shown in the right panel of Figure 4 as well. Then we define the *normalized L values*: $L_{\text{norm}} = L - L_{\text{med}}$, where L_{med} corresponding to the pixel's declination is subtracted from the original value in each pixel. Only these normalized values L_{norm} are used in other sections of this paper. Our approach to account for the effect of higher L values at higher declinations increases the robustness of results of the performed statistical analysis.

As can be seen in both panels of Figure 4 and in the map itself (Figure 1), the typical L values drop closer to zero when approaching the poles; in the Northern sky this change happens around $\delta = 75^\circ$. Nevertheless, we do not treat this area specially in any way and believe that it does not have any significant effect on any further analysis: only $\approx 3\%$ of the Northern sky is in the region $\delta > 75^\circ$.

REFERENCES

- Aartsen, M. G., et al. 2016, *Astrophys. J.*, 833, 3, doi: [10.3847/0004-637X/833/1/3](https://doi.org/10.3847/0004-637X/833/1/3)
- Aartsen, M. G., Abraham, K., Ackermann, M., et al. 2017a, *ApJ*, 835, 45, doi: [10.3847/1538-4357/835/1/45](https://doi.org/10.3847/1538-4357/835/1/45)
- . 2017b, *ApJ*, 835, 151, doi: [10.3847/1538-4357/835/2/151](https://doi.org/10.3847/1538-4357/835/2/151)
- Aartsen, M. G., Ackermann, M., Adams, J., et al. 2019a, *European Physical Journal C*, 79, 234, doi: [10.1140/epjc/s10052-019-6680-0](https://doi.org/10.1140/epjc/s10052-019-6680-0)
- . 2019b, *ApJ*, 886, 12, doi: [10.3847/1538-4357/ab4ae2](https://doi.org/10.3847/1538-4357/ab4ae2)
- . 2020a, *PhRvL*, 124, 051103, doi: [10.1103/PhysRevLett.124.051103](https://doi.org/10.1103/PhysRevLett.124.051103)
- . 2020b, *Astroparticle Physics*, 116, 102392, doi: [10.1016/j.astropartphys.2019.102392](https://doi.org/10.1016/j.astropartphys.2019.102392)
- Abdo, A. A., Ackermann, M., Agudo, I., et al. 2010, *ApJ*, 716, 30, doi: [10.1088/0004-637X/716/1/30](https://doi.org/10.1088/0004-637X/716/1/30)
- Aharonian, F., Akhperjanian, A. G., Bazer-Bachi, A. R., et al. 2006, *Science*, 314, 1424, doi: [10.1126/science.1134408](https://doi.org/10.1126/science.1134408)
- Ahlers, M., & Halzen, F. 2018, *Progress in Particle and Nuclear Physics*, 102, 73, doi: [10.1016/j.pnpnp.2018.05.001](https://doi.org/10.1016/j.pnpnp.2018.05.001)
- Albert, A., André, M., Anghinolfi, M., et al. 2020, *ApJ*, 892, 92, doi: [10.3847/1538-4357/ab7afb](https://doi.org/10.3847/1538-4357/ab7afb)
- Avrorin, A., Aynutdinov, V., Belolaptikov, I., et al. 2011, *Nuclear Instruments and Methods in Physics Research A*, 639, 30, doi: [10.1016/j.nima.2010.09.137](https://doi.org/10.1016/j.nima.2010.09.137)
- Beasley, A. J., Gordon, D., Peck, A. B., et al. 2002, *ApJS*, 141, 13, doi: [10.1086/339806](https://doi.org/10.1086/339806)
- Berezinskii, V. S., & Ginzburg, V. L. 1981, *MNRAS*, 194, 3, doi: [10.1093/mnras/194.1.3](https://doi.org/10.1093/mnras/194.1.3)
- Berezinsky, V. 1977, in *Proceedings of the Neutrino-77 Conference, Moscow*, 177

- Böttcher, M. 2019, *Galaxies*, 7, 20, doi: [10.3390/galaxies7010020](https://doi.org/10.3390/galaxies7010020)
- Bykov, A., Gehrels, N., Krawczynski, H., et al. 2012, *SSRv*, 173, 309, doi: [10.1007/s11214-012-9896-y](https://doi.org/10.1007/s11214-012-9896-y)
- Capel, F., Mortlock, D. J., & Finley, C. 2020, *PhRvD*, 101, 123017, doi: [10.1103/PhysRevD.101.123017](https://doi.org/10.1103/PhysRevD.101.123017)
- Cerruti, M. 2019, in *Proceedings of TAUP 2019*, arXiv:1912.03666. <http://taup2019.icrr.u-tokyo.ac.jp/>
- de Angelis, A., Tatischeff, V., Grenier, I. A., et al. 2018, *Journal of High Energy Astrophysics*, 19, 1, doi: [10.1016/j.jheap.2018.07.001](https://doi.org/10.1016/j.jheap.2018.07.001)
- Dermer, C. D., & Menon, G. 2009, *High Energy Radiation from Black Holes: Gamma Rays, Cosmic Rays, and Neutrinos* (Princeton University Press)
- Eichler, D. 1979, *ApJ*, 232, 106, doi: [10.1086/157269](https://doi.org/10.1086/157269)
- Fisher, R. A. 1925, *Statistical methods for research workers*
- Fomalont, E. B., Petrov, L., MacMillan, D. S., Gordon, D., & Ma, C. 2003, *AJ*, 126, 2562, doi: [10.1086/378712](https://doi.org/10.1086/378712)
- Gordon, D., Jacobs, C., Beasley, A., et al. 2016, *AJ*, 151, 154, doi: [10.3847/0004-6256/151/6/154](https://doi.org/10.3847/0004-6256/151/6/154)
- Hayashida, M., Nalewajko, K., Madejski, G. M., et al. 2015, *ApJ*, 807, 79, doi: [10.1088/0004-637X/807/1/79](https://doi.org/10.1088/0004-637X/807/1/79)
- Huber, M. 2019, in *36th International Cosmic Ray Conference (ICRC2019)*. <https://arxiv.org/abs/1908.08458>
- IceCube Collaboration. 2018, *All-Sky Point-Source IceCube Data: Years 2010-2012*, IceCube Neutrino Observatory, doi: [10.21234/B4F04V](https://doi.org/10.21234/B4F04V)
- . 2020, *All-Sky Point-Source IceCube Data: Years 2012-2015*, IceCube Neutrino Observatory, doi: [10.21234/EXM3-TM26](https://doi.org/10.21234/EXM3-TM26)
- IceCube Collaboration, Aartsen, M. G., Ackermann, M., et al. 2018a, *Science*, 361, eaat1378, doi: [10.1126/science.aat1378](https://doi.org/10.1126/science.aat1378)
- . 2018b, *Science*, 361, 147, doi: [10.1126/science.aat2890](https://doi.org/10.1126/science.aat2890)
- . 2020a, *arXiv e-prints*, arXiv:2001.09520. <https://arxiv.org/abs/2001.09520>
- . 2020b, *arXiv e-prints*, arXiv:2001.09520. <https://arxiv.org/abs/2001.09520>
- Inoue, Y., Khangulyan, D., Inoue, S., & Doi, A. 2019, *ApJ*, 880, 40, doi: [10.3847/1538-4357/ab2715](https://doi.org/10.3847/1538-4357/ab2715)
- Jorstad, S. G., Marscher, A. P., Morozova, D. A., et al. 2017, *ApJ*, 846, 98, doi: [10.3847/1538-4357/aa8407](https://doi.org/10.3847/1538-4357/aa8407)
- Katz, U. F. 2006, *Nuclear Instruments and Methods in Physics Research A*, 567, 457, doi: [10.1016/j.nima.2006.05.235](https://doi.org/10.1016/j.nima.2006.05.235)
- Kovalev, Y. Y., Petrov, L., Fomalont, E. B., & Gordon, D. 2007, *AJ*, 133, 1236, doi: [10.1086/511157](https://doi.org/10.1086/511157)
- Kovalev, Y. Y., Pushkarev, A. B., Nokhrina, E. E., et al. 2020, *MNRAS*, 495, 3576, doi: [10.1093/mnras/staa1121](https://doi.org/10.1093/mnras/staa1121)
- Kovalev, Y. Y., Kellermann, K. I., Lister, M. L., et al. 2005, *AJ*, 130, 2473, doi: [10.1086/497430](https://doi.org/10.1086/497430)
- Lemoine, M., & Waxman, E. 2009, *JCAP*, 2009, 009, doi: [10.1088/1475-7516/2009/11/009](https://doi.org/10.1088/1475-7516/2009/11/009)
- Lister, M. L., Homan, D. C., Hovatta, T., et al. 2019, *ApJ*, 874, 43, doi: [10.3847/1538-4357/ab08ee](https://doi.org/10.3847/1538-4357/ab08ee)
- Mao, P., Urry, C. M., Massaro, F., et al. 2016, *ApJS*, 224, 26, doi: [10.3847/0067-0049/224/2/26](https://doi.org/10.3847/0067-0049/224/2/26)
- Neronov, A., & Semikoz, D. 2020, *JETP*, 158, 295, doi: [10.31857/S0044451020080064](https://doi.org/10.31857/S0044451020080064)
- Neronov, A., Semikoz, D., Aharonian, F., & Kalashev, O. 2002, *PhRvL*, 89, 051101, doi: [10.1103/PhysRevLett.89.051101](https://doi.org/10.1103/PhysRevLett.89.051101)
- Neronov, A., Semikoz, D. V., & Ptitsyna, K. 2017, *A&A*, 603, A135, doi: [10.1051/0004-6361/201630098](https://doi.org/10.1051/0004-6361/201630098)
- Padovani, P., Resconi, E., Giommi, P., Arsioli, B., & Chang, Y. L. 2016, *MNRAS*, 457, 3582, doi: [10.1093/mnras/stw228](https://doi.org/10.1093/mnras/stw228)
- Palladino, A., Spurio, M., & Vissani, F. 2020, *Universe*, 6, 30, doi: [10.3390/universe6020030](https://doi.org/10.3390/universe6020030)
- Palladino, A., & Vissani, F. 2016, *ApJ*, 826, 185, doi: [10.3847/0004-637X/826/2/185](https://doi.org/10.3847/0004-637X/826/2/185)
- Palladino, A., & Vissani, F. 2017, *Astron. Astrophys.*, 604, A18, doi: [10.1051/0004-6361/201730739](https://doi.org/10.1051/0004-6361/201730739)
- Petrov, L. 2011, *AJ*, 142, 105, doi: [10.1088/0004-6256/142/4/105](https://doi.org/10.1088/0004-6256/142/4/105)
- . 2012, *MNRAS*, 419, 1097, doi: [10.1111/j.1365-2966.2011.19765.x](https://doi.org/10.1111/j.1365-2966.2011.19765.x)
- . 2013, *AJ*, 146, 5, doi: [10.1088/0004-6256/146/1/5](https://doi.org/10.1088/0004-6256/146/1/5)
- . 2017, *Transactions of IAA RAS*, 64. <http://iaaras.ru/en/library/paper/1681/>
- . 2020, *AJ submitted*, arXiv:2008.09243. <https://arxiv.org/abs/2008.09243>
- Petrov, L., de Witt, A., Sadler, E. M., Phillips, C., & Horiuchi, S. 2019, *MNRAS*, 485, 88, doi: [10.1093/mnras/stz242](https://doi.org/10.1093/mnras/stz242)
- Petrov, L., Gordon, D., Gipson, J., et al. 2009, *Journal of Geodesy*, 83, 859, doi: [10.1007/s00190-009-0304-7](https://doi.org/10.1007/s00190-009-0304-7)
- Petrov, L., Kovalev, Y. Y., Fomalont, E. B., & Gordon, D. 2005, *AJ*, 129, 1163, doi: [10.1086/426920](https://doi.org/10.1086/426920)
- . 2006, *AJ*, 131, 1872, doi: [10.1086/499947](https://doi.org/10.1086/499947)
- . 2008, *AJ*, 136, 580, doi: [10.1088/0004-6256/136/2/580](https://doi.org/10.1088/0004-6256/136/2/580)
- . 2011a, *AJ*, 142, 35, doi: [10.1088/0004-6256/142/2/35](https://doi.org/10.1088/0004-6256/142/2/35)
- Petrov, L., Phillips, C., Bertarini, A., Murphy, T., & Sadler, E. M. 2011b, *MNRAS*, 414, 2528, doi: [10.1111/j.1365-2966.2011.18570.x](https://doi.org/10.1111/j.1365-2966.2011.18570.x)
- Piner, B. G., Pushkarev, A. B., Kovalev, Y. Y., et al. 2012, *ApJ*, 758, 84, doi: [10.1088/0004-637X/758/2/84](https://doi.org/10.1088/0004-637X/758/2/84)
- Plavin, A., Kovalev, Y. Y., Kovalev, Y. A., & Troitsky, S. 2020, *ApJ*, 894, 101, doi: [10.3847/1538-4357/ab86bd](https://doi.org/10.3847/1538-4357/ab86bd)

- Popkov, A. V., Kovalev, Y. Y., Petrov, L. Y., & Kovalev, Y. A. 2020, AJ submitted, arXiv:2008.06803.
<https://arxiv.org/abs/2008.06803>
- Ptitsyna, K., & Neronov, A. 2016, A&A, 593, A8,
 doi: [10.1051/0004-6361/201527549](https://doi.org/10.1051/0004-6361/201527549)
- Pushkarev, A. B., Hovatta, T., Kovalev, Y. Y., et al. 2012, A&A, 545, A113, doi: [10.1051/0004-6361/201219173](https://doi.org/10.1051/0004-6361/201219173)
- Pushkarev, A. B., & Kovalev, Y. Y. 2012, A&A, 544, A34,
 doi: [10.1051/0004-6361/201219352](https://doi.org/10.1051/0004-6361/201219352)
- Pushkarev, A. B., Kovalev, Y. Y., & Lister, M. L. 2010, ApJL, 722, L7, doi: [10.1088/2041-8205/722/1/L7](https://doi.org/10.1088/2041-8205/722/1/L7)
- Pushkarev, A. B., Kovalev, Y. Y., Lister, M. L., & Savolainen, T. 2017, MNRAS, 468, 4992,
 doi: [10.1093/mnras/stx854](https://doi.org/10.1093/mnras/stx854)
- Righi, C., Tavecchio, F., & Pacciani, L. 2019, Mon. Not. Roy. Astron. Soc., 484, 2067, doi: [10.1093/mnras/sty3072](https://doi.org/10.1093/mnras/sty3072)
- Schinzel, F. K., Petrov, L., Taylor, G. B., et al. 2015, ApJS, 217, 4, doi: [10.1088/0067-0049/217/1/4](https://doi.org/10.1088/0067-0049/217/1/4)
- Shu, F., Petrov, L., Jiang, W., et al. 2017, ApJS, 230, 13,
 doi: [10.3847/1538-4365/aa71a3](https://doi.org/10.3847/1538-4365/aa71a3)
- Sikora, M., Kirk, J. G., Begelman, M. C., & Schneider, P. 1987, ApJL, 320, L81, doi: [10.1086/184980](https://doi.org/10.1086/184980)
- Sironi, L., & Spitkovsky, A. 2009, ApJ, 698, 1523,
 doi: [10.1088/0004-637X/698/2/1523](https://doi.org/10.1088/0004-637X/698/2/1523)
- Smolčić, V., Zamorani, G., Schinnerer, E., et al. 2009, ApJ, 696, 24, doi: [10.1088/0004-637X/696/1/24](https://doi.org/10.1088/0004-637X/696/1/24)
- Smolčić, V., Novak, M., Delvecchio, I., et al. 2017, A&A, 602, A6, doi: [10.1051/0004-6361/201730685](https://doi.org/10.1051/0004-6361/201730685)
- Stettner, J. 2019, in International Cosmic Ray Conference, Vol. 36, 36th International Cosmic Ray Conference (ICRC2019), 1017. <https://arxiv.org/abs/1908.09551>
- Woo, J.-H., & Urry, C. M. 2002, ApJ, 579, 530,
 doi: [10.1086/342878](https://doi.org/10.1086/342878)
- Yuan, C., Murase, K., & Mészáros, P. 2020, ApJ, 890, 25,
 doi: [10.3847/1538-4357/ab65ea](https://doi.org/10.3847/1538-4357/ab65ea)